



Enhancement of Pool Boiling Heat Transfer Through Micro-Finned Surfaces and Al_2O_3 -Water Nanofluids: A Numerical Study



Hamzah Hadi Fadhl¹, Laith Jaafer Habeeb^{2*} 

¹ Mechanical Engineering Department, Faculty of Engineering, Shahid Chamran University of Ahvaz, 61000 Ahvaz, Iran

² Training and Workshop Center, University of Technology- Iraq, 10001 Baghdad, Iraq

* Correspondence: Laith Jaafer Habeeb (Laith.J.Habeeb@uotechnology.edu.iq)

Received: 12-18-2023

Revised: 02-29-2024

Accepted: 03-05-2024

Citation: H. H. Fadhl and L. J. Habeeb, "Enhancement of pool boiling heat transfer through micro-finned surfaces and Al_2O_3 -water nanofluids: A numerical study," *J. Sustain. Energy*, vol. 3, no. 1, pp. 30–45, 2024. <https://doi.org/10.56578/jse030103>.



© 2024 by the author(s). Published by Acadlore Publishing Services Limited, Hong Kong. This article is available for free download and can be reused and cited, provided that the original published version is credited, under the CC BY 4.0 license.

Abstract: Among the various heat transfer mechanisms, boiling heat transfer is distinguished by its capacity to dissipate substantial heat via the latent heat of vaporization with minimal temperature differentials. This phenomenon is pivotal across a range of industrial applications, including the cooling of macro- and micro-electronic devices, boiler tubes in power generation plants, evaporators in refrigeration systems, and nuclear reactors, where the nucleate pool boiling regime and two-phase flow are of particular interest. The drive to enhance heat exchange systems' efficiency has consistently focused on minimizing heat loss through system miniaturization. This investigation employs numerical simulations via the Fluent software to elucidate the heat transfer and cooling processes facilitated by nanofluids with varied concentrations on differently shaped finned surfaces, alongside the utilization of water and ethylene glycol as base fluids. Specifically, the thermal performance of Al_2O_3 -water nanofluids at different concentrations (0, 0.3, 0.6, 1, 1.2, and 1.4 percent by volume) was scrutinized under boiling conditions across surfaces endowed with circular, triangular, and square fins. The study confirmed that the incorporation of Al_2O_3 nanoparticles into the water base fluid not only enhances its thermal conductivity but, in conjunction with micro-finned surfaces, also augments the available surface area, thereby improving wettability. These modifications collectively contribute to a marked increase in the heat transfer coefficient (HTC) and a reduction in the critical heat flux (CHF). Furthermore, it was observed that at a 0.3% volume concentration of Al_2O_3 with square fins, the temperature span extends from 373.1 to 383.1 K. Nonetheless, the long-term stability and efficacy of nanofluids are subject to potential impacts from nanoparticle aggregation and sedimentation. This study underlines the synergistic effect of nanoparticle-enhanced fluids and micro-finned surface architectures in bolstering pool boiling heat transfer, signifying a promising avenue for thermal management advancements in various industrial domains.

Keywords: Aluminum oxide (Al_2O_3); Nanofluids; Heat transfer enhancement; Pool boiling; Micro-finned surfaces; Numerical simulation

1 Introduction

In high-heat-flux components such as electronic devices like computers, pool boiling is an attractive approach for cooling applications. Due to the superior heat rate as a result of the phase change phenomenon, boiling has widely been used as a dominant heat transfer mechanism in two-phase thermal systems. This intensifying heat transfer performance during the boiling process is essential for saving energy and keeping those systems durable. In previous research, the problem was addressed by many researchers, but the high costs of nanofluids led to the experiments being economically costly. In this study, numerical simulations (fluent) were used to predict the phenomenon of heat transfer and cooling processes, which gives a greater opportunity to test the use of more concentrations of nanofluid, as well as the use of different geometric shapes for the fins, as well as experimenting with more than one base fluid with nanofluids at a lower cost.

Salehi and Hormoz [1] studied the HTC of Al_2O_3 -water nanofluids with modest heat fluxes in a nucleate pool in 2018. The device was constructed to investigate the HTC in a boiling nucleate pool. Al_2O_3 nanoparticles were dispersed in clean water, and the nanofluids were stabilized. Numerical simulations and the Eulerian two-phase

approach have been used, and experimental correlations are used to predict bubble parameters. Using the response surface approach, a prediction equation for the nanofluid's HTC has been suggested. The factors examined are the distance from the center of the boiling surface, the applied heat flux, the density of nucleation sites, the bubble frequency, and the bubble departure diameter. The HTC was determined utilizing simulation and experimental data, as well as Bahrami's [2] and numerical methods.

The heat transmission during pool boiling on a miniature surface covered with nanostructure was investigated in 2015 by Strak et al. [3] Incorporating carbon nanotubes (CNTs) onto a surface improves heat transport and decreases superheat incipient. The experiment compared three different surfaces that can transfer the heat of boiling water: surfaces that are coated with CNTs (MF+N) surface code (minfins with carbon nanotubes), surfaces that are formed by sintering a woven copper wire mesh to the tips of minfins (MF+M minfins), and surfaces that are coated with nanotubes alone (MF) together with two scalding liquids—ethyl alcohol and water. The researchers set out to identify the most effective liquids and tested surfaces for electronic device cooling, as well as those surfaces that may serve as heat sinks or heat tube evaporators. Here are the key takeaways from the outcome:

- (1) The mesh-covered minifins improved boiling heat transfer coefficients for both water and ethyl alcohol at low and medium heat fluxes the most, which is likely due to the high concentration of active nucleation sites.
- (2) At high heat fluxes, the surface covered with CNTs improved boiling heat transfer coefficients for both water and ethyl alcohol the most.
- (3) Compared to the surface with wire mesh, the one with CNTs significantly increases the CHF at ethyl alcohol boiling, around 3.5 times.

(4) In both water and ethyl alcohol, the plain mini-fins surface showed the lowest HTC. Rahman and McCarthy [4], in 2017, used two heterogeneous surface designs combining the elements of nanostructures, mixed wettability, and bi-conductivity to study the effects of nano-structured coatings, mixed wettability, and binary conductivity on saturated pool boiling of water at atmospheric pressure conditions. Putting these different enhancement methods together has been shown to make CHF and HTC 2.5 times and 10 times higher than on copper surfaces that are not enhanced.

Kumar et al. [5] studied a hollowed copper cylinder with an outer diameter of 25 mm and a length of 40 mm as the working fluid to enhance pool boiling heat transfer coefficient (PBHTC). A screen-printing method was employed to produce heterogeneous wettable structures on a copper surface. It assessed the effects on boiling heat transfer efficiency and bubble dynamics of heterogeneous wettable surfaces with different line pattern inclination angles. We examined interlaced line designs with 0° , 30° , 60° , and 90° inclinations. The findings showed that interlaced patterns with an angle of $\theta = 30^\circ$ and $\theta = 60^\circ$ have a big impact on heat transfer coefficients, which were 89.27%, 104.59%, 103.99%, and 71.65%, in that order.

In 2009, Kim et al. [6] studied the quenching media of water-based nanofluids by using alumina, silica, and diamond nanoparticles with mixing ratios less than 0.1 vol%, and the characteristics of the quenching process of the spherical probe steel (10 mm diameter) made from stainless steel used in the experiment. The results showed that the CHF and minimum heat flux depend on the nanoparticle type used in the experiment.

Ciloglu and Bolukbasi [7] studied the effect of water nanofluids on their quenching properties. Probes made from brass with a diameter of 20 mm and a length of 75 mm were quenched in water and water nanofluids (Al_2O_3 , SiO_2 , TiO_2 , and CuO). The results showed that the addition of nanoparticles to water enhances the surface properties due to the porous layer of nanoparticles formed on the surface during the cooling process, where increased wettability was observed, resulting in increased heat transfer and improving the quenching process. It also showed water-based (SiO_2) nanofluids were better than other species used, resulting in a decrease in contact angle and an increase in adhesion intensity, which, in turn, prevents the growth of bubbles around the surface.

Akbar et al. [8] investigated the boiling of saturated pools of distilled water under atmospheric pressure, using copper substrates coated with a new industrial nanofluid containing silver nanoparticles (Nano Coolant) at two distinct concentrations. We examined the surfaces' microstructure, topography, and contact angle. On the re-entrant inclined little channel, the optimum concentration with hydrophobic properties was deposited. We compared pool boiling curves and investigated the impact of reentrancy and hydrophobicity on bubble dynamics. Cluster deposition and hydrophobicity increased with increasing nanoparticle concentrations, although the stability of the deposition diminished. The results of the experiments showed that increasing the concentration of the nanofluid until it reached the polished nanocoated surface increased the CHF and HTC of pool boiling. Nano-fins are offered as a revolutionary method of increasing heat transfer. When compared to polished copper, it was shown that inclination and reentrancy enhance pool boiling performance. Lastly, as anticipated, the combined modification yields the highest CHF and HTC values of 196 W/cm^2 and $10 \text{ W/cm}^2 \text{ K}$, respectively, compared to the plain surface. This modification entails coating the surface with silver nanoparticles deposited on the internal side of the re-entrant inclined minichannel.

This study focuses on two enhancements to enhance pool boiling heat transfer and improve thermal management in high heat flux components. Nanofluids and micro-finned surfaces are chosen based on their potential to address key challenges associated with conventional cooling techniques and their compatibility with pool boiling applications. Nanofluids offer the potential to improve thermal properties such as thermal conductivity and convective heat transfer

coefficients, while micro-finned surfaces provide increased surface area and alter surface wettability. The study aims to exploit the synergistic effects of these enhancements to achieve significant improvements in pool boiling heat transfer.

Other researchers [9–14] studied nanofluids and boiling heat transfer for different applications, boundary conditions, geometries, configurations, based nanofluids, nanoparticles, and range of parameters. They concluded that when adding nanoparticles to base fluid, heat transfer enhanced clearly.

Research into the effects of working fluid, surface modification, and heat transfer in a pool is the focus of this research. Recent developments in microsystems have made it possible for many electronic devices to increase their processing capacity while simultaneously decreasing their size. However, such devices dramatically enhance the amount of heat dissipated per unit area. Moreover, improving the HTC by using nanofluid (Al_2O_3) with different concentrations. In addition, use of surfaces containing circular, triangular, and square-shaped fins and use of two types of base fluids (water).

2 Theoretical Details

Boiling is the process of converting liquid into vapor by adding heat from an external source (phase change) [15]. The vapor bubbles occur either on the heated surface itself or in a superheated liquid layer close to it. While boiling is a difficult and elusive process, it is a very efficient mechanism of heat transmission in a variety of energy conversion and heat exchange systems, as well as for cooling high-energy-density electronic components. There are two forms of boiling that are often used: pool boiling and flow or forced convective boiling. The flow boiling is boiling in a flowing stream of fluid, where the heating surface may be the channel wall confining the flow, while the term "pool boiling" refers to the process of boiling on a heated surface (warmer) immersed in a pool of originally dormant liquid. Heat flux in any boiling process is a critical element in designing and running high-temperature heat transfer equipment such as boilers, evaporators, electronic equipment, and rocket engines. When a pool boils, the fluid initially remains stationary at the heating surface, and subsequent fluid motion is caused by free convection, bubble expansion, and detachment-induced circulation. Table 1 shows the properties of nanofluid Al_2O_3 -water.

Table 1. Properties of nanofluid Al_2O_3 -water

	Water	Nanofluid Al_2O_3 -Water				
		Con. 0.3%	Con. 0.6%	Con. 1%	Con. 1.2%	Con. 1.4%
K	0.613	0.608033942	0.60309463	0.59655012	0.5932954	0.5896657
ρ	999	1005.919	1014.838	1026.730	1032.676	1038.6219
c_p	4217	4168.038	4157.076	4142.460	4127.8438	4135.1519

The term "subcooled boiling" describes a physical situation where the wall temperature is high enough to cause boiling at the wall even while the average temperature of the liquid in the bulk is lower than the saturation point. Under these conditions, the energy is transferred to the liquid from the wall in an instant. Some of the energy will be converted into vapor, while some will be used to raise the temperature of the liquid. The average liquid temperature will also increase due to interphase heat transfer, but saturated vapor will condense. In addition, it's possible that some of the energy goes straight from the wall into the vapor. The models developed at the Rensselaer Polytechnic Institute (RPI) are based on these essential processes [16]. When it comes to wall boiling models, there are three separate wall boundary conditions that work: isothermal wall, specified heat flow, and stated coefficient of heat transfer (coupled wall boundary). The three common wall boundary conditions in heat transfer modeling are isothermal walls, specified heat flow, and stated coefficients of heat transfer. An isothermal wall requires the temperature of the wall to remain constant, while a specified heat flow specifies the rate of heat flux into or out of the wall. The stated coefficient of heat transfer defines the HTC between the wall and the fluid and is influenced by factors such as fluid properties, flow conditions, and surface geometry. Past work has shown the presentation of turbulence models in boiling flows and specialized submodels for interfacial momentum, mass, and heat transfers.

2.1 Assumptions

The following assumptions are used in the model:

- (1) Transient two-dimensional flow in the working fluid with a single-phase fluid (homogenous model).
- (2) Incompressible and Newtonian fluid.
- (3) The kinetic and potential energy changes are negligible.
- (4) No heat generation within the enclosure.
- (5) The effective thermophysical properties are assumed to be dependent on the concentration of the nanoparticles.
- (6) No chemical reaction between nanoparticles and the base fluid.

2.2 RPI Model

The basic RPI model separates the total heat flux from the wall to the liquid into three components: convective heat flux, quenching heat flux, and evaporative heat flux.

Convective heat flux refers to the rate of heat transfer between a surface and a fluid due to convection, where the fluid motion plays a significant role in heat transfer. It represents the amount of heat transferred per unit area per unit time.

Quenching heat flux is the maximum heat flux at which a surface can be cooled by a boiling liquid before it reaches a critical temperature. Beyond this heat flux, the surface temperature increases rapidly due to insufficient cooling.

Evaporative heat flux is the heat flux associated with the phase change of a liquid to vapor during boiling. It represents the amount of heat required to vaporize the liquid per unit area and per unit time.

$$\dot{q}_W = \dot{q}_C + \dot{q}_Q + \dot{q}_E \quad (1)$$

The heated wall surface is separated into sections called area A_b , which is covered by nucleating bubbles and a portion $(1 - A_b)$, which is covered by the fluid.

The convective heat flux \dot{q}_C is expressed as:

$$\dot{q}_C = h_c (T_w - T_1) (1 - A_b) \quad (2)$$

where, h_c is the single-phase heat transfer coefficient, and T_w and T_1 are the wall and liquid temperatures, respectively.

The quenching heat flux \dot{q}_Q models the cyclic averaged transient energy transfer related to liquid filling the wall vicinity after bubble detachment, and is expressed as:

$$\dot{q}_Q = \frac{2k_l}{\sqrt{\pi \lambda_l T}} (T_w - T_l) \quad (3)$$

where, k_l is the conductivity, T is the periodic time, and $\lambda_l = \frac{k_l}{\rho_l C_p l}$ is the diffusivity. The evaporative flux \dot{q}_E is given by:

$$\dot{q}_E = V_d N_w \rho_v h_{fv} f \quad (4)$$

where, V_d is the volume of the bubble based on the bubble departure diameter, N_w is the active nucleate site density, ρ_v is the vapor density, and h_{fv} is the latent heat of evaporation, and f is the bubble departure frequency. These equations need closure for the following parameters:

2.3 Area of Influence

Its definition is based on the departure diameter and the nucleate site density:

$$A_b = K \frac{N_w \pi D_w^2}{4} \quad (5)$$

It should be noted that in order to avoid numerical instability produced by unbound nucleate site density empirical correlations, the area of influence must be constrained. The following is the impact zone:

$$A_b = \min \left(1, K \frac{N_w \pi D_w^2}{4} \right) \quad (6)$$

While it is customary to fix the empirical constant K to 4, it has been shown to be non-universal, ranging between 1.8 and 5. Additionally, based on Del Valle and Kenning's results, the following connection has been added for this constant:

$$K = 4.8 e^{\left(-\frac{J a_{\text{sub}}}{80} \right)} \quad (7)$$

And $J a_{\text{sub}}$ is the subcooled Jacob number defined as:

$$J a_{\text{sub}} = \frac{\rho_l C_{pl} \Delta T_{\text{sub}}}{\rho_v h_{fv}} \quad (8)$$

where, $\Delta T_{\text{sub}} = T_{\text{sat}} - T_l$.

2.4 Frequency of Bubble Departure

Common methods for putting the RPI concept into practice include: Similar to inertia-controlled expansion, bubble deflation occurs at a regular interval (not really applicable to subcooled boiling).

$$f = \frac{1}{T} = \sqrt{\frac{4g(\rho_l - \rho_v)}{3\rho_l D_w}} \quad (9)$$

2.5 Nucleate Site Density

Usually, the density of nucleate sites is expressed by a correlation based on the wall superheat. The colloquial term is of the following form:

$$N_w = C^n (T_w - T_{\text{sat}})^n \quad (10)$$

The empirical parameters proposed by Lemmert and Chawla are used here with $n=1.805$ and $C=210$. You may also get it in other forms, such as Ishii and Kocamustafaogullari.

$$N_w^* = f(\rho^*) r_c^* - 4.4 \quad (11)$$

Here, $N_w^* = N_w D_w^2$, $r_c^* = 2r_c/D_w$, $r_c = \frac{2\sigma T_{\text{sat}}}{\rho_v h_{fv} \Delta T_W}$, $\rho^* = (\rho_l - \rho_v) / \rho_v$. where, D_w is the bubble's diameter at its starting position, and the density function is defined as:

$$f(\rho^*) = 2.157 \times 10^{-7} \rho^{*-3.2} (1 + 0.0049\rho^*)^{4.13} \quad (12)$$

2.6 Bubble Departure Diameter

The default bubble departure diameter in meters is calculated using empirical correlations in the RPI model.

$$D_w = \min(0.0014, 0.0006e^{-\Delta T_{\text{sub}}/45.0}) \quad (13)$$

while Kocamustafaogullari and Ishii use

$$D_w = 0.0012 (\rho^*)^{0.9} 0.0208 \theta \sqrt{\frac{\sigma}{g(\rho_l - \rho_v)}} \quad (14)$$

with the contact angle expressed in degrees. The other relationship is used to calculate the bubble departure diameter in millimeters.

$$D_w = 2.4210^{-5} p^{0.709} \left(\frac{a}{b\sqrt{\varphi}} \right) \quad (15)$$

$$a = \frac{\Delta T_{\text{sup}}}{2\rho_g H_{lv}} \sqrt{\frac{\rho_s C_{ps} k_S}{\pi}} \quad (16)$$

$$b = \begin{cases} \frac{\Delta T_{\text{sub}}}{2(1 - \frac{\rho_g}{\rho_l})} e^{\left(\frac{\Delta T_{\text{sub}}}{3} - 1\right)} & \Delta T_{\text{sub}} \leq 3 \\ \frac{\Delta T_{\text{sub}}}{2(1 - \frac{\rho_g}{\rho_l})} & \Delta T_{\text{sub}} > 3 \end{cases} \quad (17)$$

$$\varphi = \max \left(\left(\frac{U_b}{U_0} \right)^{0.47}, 1.0 \right) \quad (18)$$

where, the flow pressure is denoted as P , $\Delta T_{\text{sub}} = T_w - T_{\text{sat}}$ is the wall superheat, H_{lv} is the latent heat, U_b is the near wall bulk velocity, and $U_b=0.61\text{m/s}$. The solid, liquid, and gas phases are represented by the subscripts s, l, and g, respectively.

2.7 Non-Equilibrium Sub Cooled Boiling

When using the basic RPI model, the vapor's temperature is not determined but is set at its saturation temperature. To denote boiling that occurs outside of the nucleate boiling regime Departure from Nucleate Boiling (DNB), or up to the CHF and post-dry-out state, the vapor temperature must be included in the solution process. The following modifications have been made to the wall heat partition:

$$\dot{q}_W = (\dot{q}_C + \dot{q}_Q + \dot{q}_E) f(\alpha_l) + (1 - f(\alpha_l)) \dot{q}_V + \dot{q}_G \quad (19)$$

where, \dot{q}_C , \dot{q}_Q , and \dot{q}_E are the convective heat fluxes in the liquid phase, the quenching heat fluxes, and the evaporation heat fluxes, respectively. The additional heat fluxes are \dot{q}_V for the vapor phase's convective heat flow and \dot{q}_G for any other conceivable gas phases in a system. That may be stated as follows:

$$\dot{q}_V = h_V (T_W - T_V) \quad (20)$$

$$\dot{q}_G = h_G (T_W - T_G) \quad (21)$$

As with the liquid phase \dot{q}_G , the convective heat transfer coefficients h_V and h_G are determined using wall function formulas.

$f(\alpha_l)$ is proportional to the fraction of local liquid volume and has the same limiting points as the liquid volume fraction. The following phrase was suggested by Lavieville et al.:

$$f(\alpha_l) = \begin{cases} 1 - \frac{1}{2} e^{-20(\alpha_l \alpha_{l,crit})} & \alpha_l \geq \alpha_{l,crit} \\ \frac{1}{2} \left(\frac{\alpha_l}{\alpha_{l,crit}} \right)^{20\alpha_{l,crit}} & \alpha_l < \alpha_{l,crit} \end{cases} \quad (22)$$

The crucial value for the liquid fraction is $\alpha_{l,crit} = 0.2$ in this case.

2.8 Wall Heat Flux Partition

The heat partitioning at the wall is defined in a manner analogous to that of Eq. (23), with the exception of the function specification. In this context, the function $f(\alpha_l)$ is contingent upon the local volume fractions of liquid and vapor, which are quantified as either zero or one. This characterization is based on a method that considers the local conditions of phase distribution.

$$f(\alpha_l) = \begin{cases} 1 - \frac{1}{2} \exp[-20(\alpha_l - \alpha_{l,crit})] & \alpha_l \geq \alpha_{l,crit} \\ \frac{1}{2} \left(\frac{\alpha_l}{\alpha_{l,crit}} \right)^{20\alpha_{l,crit}} & \alpha_l < \alpha_{l,crit} \end{cases} \quad (23)$$

The critical value for the liquid volume fraction is 0.2, and for the vapor phase, it is $\alpha_{v,crit} = 1 - \alpha_{l,crit} = 0.8$. The wall heat flux division, which serves to define wall boiling regimes, may also be defined using other functions:

$$f(\alpha_v) = 1 - f(\alpha_l) = \begin{cases} 0 & \alpha_v < \alpha_{v,1} \\ \frac{1}{2} \left(1 - \cos \left(\pi \frac{\alpha_v - \alpha_{v,1}}{\alpha_{v,2} - \alpha_{v,1}} \right) \right) & \alpha_{v,1} \leq \alpha_v \leq \alpha_{v,2} \\ 1 & \alpha_v > \alpha_{v,2} \end{cases} \quad (24)$$

A linear function was employed to adapt Eq. (24) for the Critical Heat Flux (CHF), considering the influence of thin film boiling.

$$f(\alpha_v) = \max \left(0, \min \left(\frac{\alpha_v - \alpha_{v,1}}{\alpha_{v,2} - \alpha_{v,1}}, 1 \right) \right) \quad (25)$$

where, the breakpoints have been set to $\alpha_{v,1} = 0.9$ and $\alpha_{v,2} = 0.95$.

The default formulation for the wall heat flow partition in ANSYS Fluent is Eq. (25).

2.9 Flow Regime Transition

The transition from nucleate boiling to the CHF and post-drying conditions causes a shift in the multiphase flow regime from bubbly to mist as wall boiling advances. So, the liquid phase becomes a dispersed state, and the vapor phase becomes a continuous state. This change in flow regime affects several parameters, including the size of the interface, the amounts of turbulence and heat transfer, and the dynamics of momentum transfer.

A long time ago, sub-channel one-dimensional thermal-hydraulic algorithms were As a means of simulating the change in flow regime and computing interfacial transfers, so-called flow regime maps are constructed using cross-section averaged flow parameters. Adding a cell-based interfacial surface topology to flow regime maps in Computational Fluid Dynamics (CFD) solvers allows us to determine the transitions between flow regimes using local flow parameters. The ensemble of all computational cells, which usually have simple local interfacial surface topologies, may produce complex global topologies, similar to how traditional sub-channel flow regime maps show the various flow regimes.

The method begins by switching from a configuration of continuous liquid bubble flow to one of continuous vapor droplet flow by making use of a simple local interfacial surface topology. The computational cell is designed to accommodate a multi-interface surface topology, and the α_v vapor volume fraction is the only local flow quantity that controls the flow regimes.

The vapor phase is distributed throughout the continuous liquid as bubbles in a bubbly flow topology. Typically $\alpha_v \leq 0.3$.

Topology of mist flow: droplets of liquid phase are scattered throughout the continuous vapor. Typically $\alpha_v \geq 0.7$.

A topology that falls somewhere in the middle between bubbly and mist flow is churn flow, where $0.3 < \alpha_v > 0.7$.

To calculate the area between the surfaces and the amounts of momentum and heat transferred across them, one uses the topologies of the surfaces that form the interfaces. The following generic form is used to compute the interfacial quantities (such as drag, lift, turbulent drift force, and heat transfer), which are represented by φ

$$\varphi = (1 - f(\alpha_v)) \varphi_{\text{bubbly}} + f(\alpha_v) \varphi_{\text{droplet}} \quad (26)$$

where, $f(\alpha_v)$ is computed using Eq. (24) or Eq. (25), but with distinct lower and upper breakpoint limitations. Typically, 0.3 and 0.7 are employed, with φ_{bubbly} and φ_{droplet} denoting the interfacial amounts associated with bubbly and mist flow, respectively.

It is worth noting that the liquid in boiling models is often described as the first phase, while the vapor is designated as the second. Once specified, it stays constant throughout flow regime transitions. However, when the variables φ_{bubbly} and φ_{droplet} are computed, the main and secondary phases are flipped. In the case of φ_{bubbly} , the liquid is considered the main phase, while the vapor is considered the secondary phase. In contrast, with the φ_{droplet} , the vapor becomes the dominant phase, while the liquid becomes the secondary phase.

3 Validation

The results were validated by comparing them with the previous results of another study that was re-run through the CFD program. The results obtained were close to the results obtained in the previous study. The previous study included the use of Al₂O₃-water nanofluids for enhancement. Using response surface methods, determine the pool boiling HTC at low heat fluxes. Salehi and Hormoz [1] studied how the Eulerian two-phase method has been applied and numerical simulation and experimental correlations are used to predict bubble parameters. The following are the dimensions of the test pool, boundary conditions, and one of the solution parameters. The computational domain was drawn in two dimensions, with a width of 200 mm and a height of 100 mm. The boiling surface has a diameter of 11 mm (Figure 1 and Figure 2). The range of heat flux tested was 30-200 kW/m², and the properties of the Al₂O₃-water nanofluid (0.3 mass%) used were: nucleation site density = 28 l/m² and departure frequency = 30 l/m². Among the bubble parameters, nucleation site density was the most impressive variable, while bubble departure diameter was the least effective variable. Control volume is used for discretization, QUICK for convective expressions, and SIMPLE for velocity-pressure coupling. Coverage criteria for continuity, momentum, and energy equations are less than 10⁻⁶. Mesh independence was tested by calculating the pool boiling heat transfer coefficient. Grid independence is achieved at 100×160 cells with q = 50 kW/m².

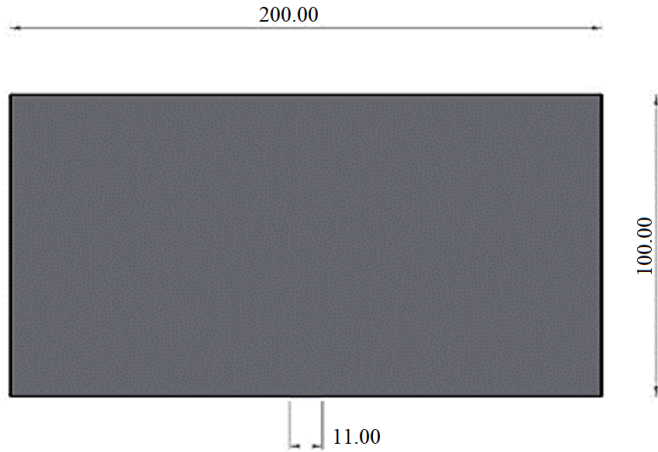


Figure 1. The dimensions of geometry

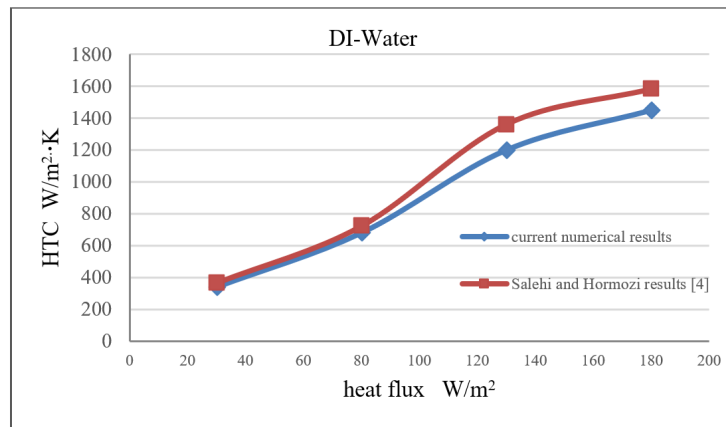


Figure 2. Comparison HTC of current numerical results with Salehi and Hormozi's results [1]

4 Result and Discussion

In this study, using numerical simulation (CFD) to find out the phenomena related to heat transfer, the total time used in these simulations was five seconds, and nanofluids were added to the cooling base fluid, where two types of these liquids were used: distilled water and Alumina was used as a nanomaterial, and five concentrations of this material were used with water coolant (0, 0.3, 0.6, 1, 1.2, 1.4% volume).

The results obtained will be reviewed as follows:

(1) Concentration of nanofluids. The use of nanomaterials in a general way to form a layer on the surface that reduces the formation of bubbles and continuously wets the surface, thus improving the HTC and thus keeping a constant temperature for the electronic devices in which these nanomaterials are used to improve cooling.

(2) Shape of fins. As for the geometric shapes used in the mesh, which were compared, there are three types: square, circular, and rectangular shapes. The system geometry in the present work consists of an integral micro-finned enclosure where the working fluid is exposed to high temperatures. Consider the problem of nanofluids inside a finned enclosure with a length of 37.5 mm and a height of 20 mm. Three types of fins are used, which are triangular, circular, and square. The height and base of triangular, the diameter of circular, and the width and height of square fins have the same dimensions of 0.3 mm, as shown in Figure 3.

A 2D geometry was created, then structured and unstructured meshes were formed. It's woven into several nodes and components, as seen in Figure 4 and Table 2.

For the computational model, the geometry is generated by using SolidWorks software to build the domain of fluid as a two-dimensional model.

(3) Water as a base fluid was used in the production of nanofluids in addition to other factors for which it has advantages, the most important of which is that it is available and cheap and has good properties for transferring heat and cooling. The properties are shown in Table 3.

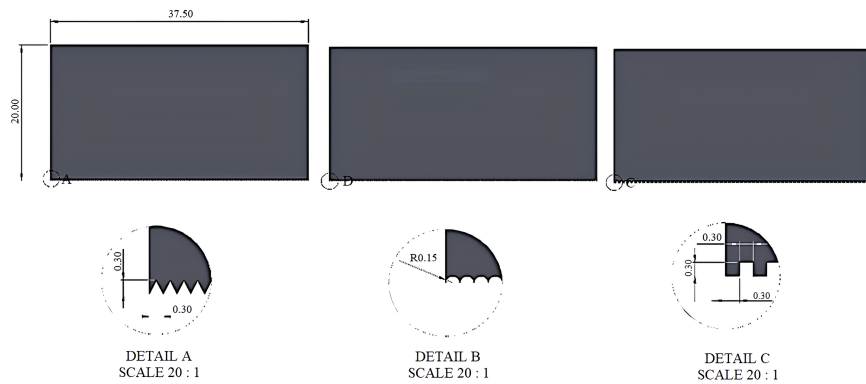


Figure 3. Physical geometry of finned enclosure

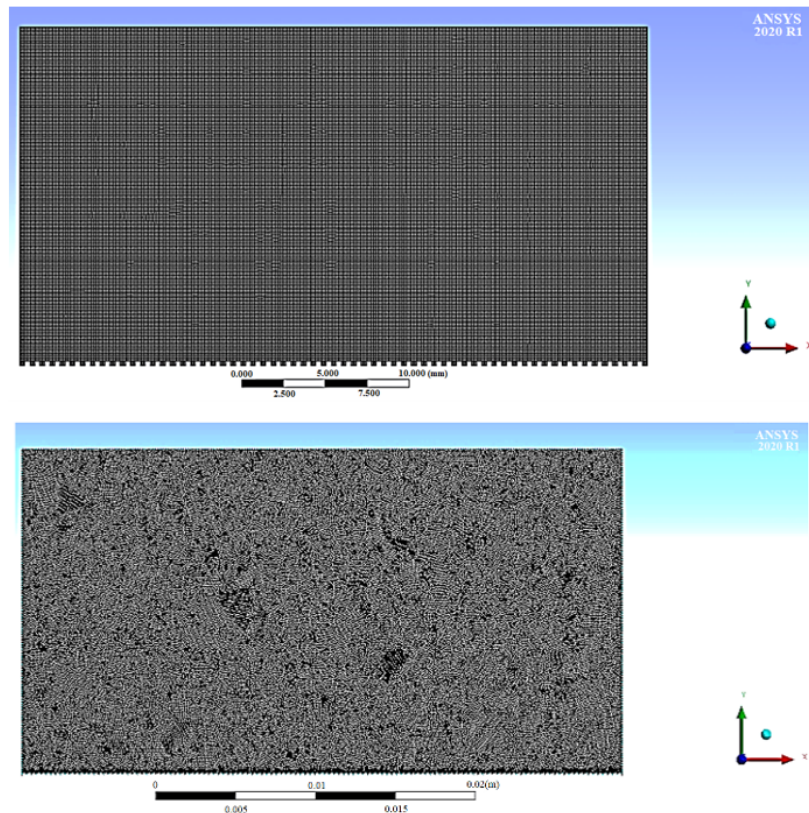


Figure 4. Meshing geometry created by ansys-workbench

Table 2. Nodes and elements for the three fins type

Fins Type	No. of Nodes	No. of Elements
Square	75204	74442
Circular	80989	159945
Triangular	75387	74669

Table 3. Properties of base fluid

Fluid	Formula	Density (g/m ³)	Specific Heat (Cp) (J/kg.K)	Boiling Point (°C)	Viscosity (kg/m.s)	Thermal Conductivity (k) (W/m.K)
Water	H ₂ O	999	4181	100	0.001	0.6

4.1 Concentration of Nanofluids

In case of this type of nanomaterials, five different concentrations were used, and the results are shown in Table 4.

Table 4. The different concentrations of nanofluids (Al_2O_3 +water) on surfaces with circular shape of fins

Circular Shape of Fins	Water	Water+ $\text{Al}_2\text{O}_3(0.3)$	Water+ $\text{Al}_2\text{O}_3(0.6)$	Water+ $\text{Al}_2\text{O}_3(0.1)$	Water+ $\text{Al}_2\text{O}_3(0.12)$	Water+ $\text{Al}_2\text{O}_3(0.14)$
HTC($\text{kW}/\text{m}^2 \cdot \text{K}$)	0.900189	0.9752501	1.2263713	0.891424	0.91140131	0.885967
$q''(\text{kW}/\text{m}^2)$	85.5089	83.14	116.49299	84.676	86.574	84.158
$V(\text{m}/\text{s})$	0.0022549	0.0021974	0.0026819	0.0024298	0.0021962	0.0024976
$P(\text{Pascal})$	191.044	192.4198	194.74019	196.635	197.81996	198.64769
$CP(\text{J}/\text{kg} \cdot \text{K})$	4179	4168.038	4157.075	4142.459	4135.1519	4127.8438
$k(\text{W}/\text{m} \cdot \text{K})$	0.612716	0.608	0.60275114	0.5960329	0.5932954	0.5896657
$\rho(\text{kg}/\text{m}^3)$	999	1005.919	1014.838	1026.73	1032.676	1038.6219

In Table 4, we note an increase in the value of HTC with a circular shape of fins at a concentration of 0.6% volume, and after that, the value of HTC decreases.

In Table 5, we note an increase in the value of HTC with a triangular shape of fins at a concentration of 0.3% volume.

Table 5. The different concentrations of nanofluids (Al_2O_3 +water) on surfaces with triangular shape of fins

Triangular Shape of Fins	Water	Water+ $\text{Al}_2\text{O}_3(0.3)$	Water+ $\text{Al}_2\text{O}_3(0.6)$	Water+ $\text{Al}_2\text{O}_3(0.1)$	Water+ $\text{Al}_2\text{O}_3(0.12)$	Water+ $\text{Al}_2\text{O}_3(0.14)$
HTC ($\text{kW}/\text{m}^2 \cdot \text{K}$)	0.799705	0.9094011	0.9016265	0.9037847	0.8097116	0.795947
$q''(\text{kW}/\text{m}^2)$	75.964	86.384	85.6455	85.8505	76.9145	75.607
$V(\text{m}/\text{s})$	0.1368468	0.0026517	0.0027019	0.0026517	0.0026517	0.0038164
$P(\text{Pascal})$	189.9451	192.733	193.601	196.4175	192.733	198.78697
$CP(\text{J}/\text{kg} \cdot \text{K})$	4179	4168.038	4157.076	4142.46	4135.1519	4127.8442
$k(\text{W}/\text{m} \cdot \text{K})$	0.61281	0.608	0.60309	0.5965501	0.5932954	0.59005231
$\rho(\text{kg}/\text{m}^3)$	999	1005.919	1014.838	1026.73	1032.676	1038.6219

In Table 6, we note an increase in the value of HTC with a square shape of fins at a concentration of 0.6% volume.

Table 6. The different concentrations of nanofluids (Al_2O_3 +water) on surfaces with square shape of fins

Square Shape of Fins	Water	Water+ $\text{Al}_2\text{O}_3(0.3)$	Water+ $\text{Al}_2\text{O}_3(0.6)$	Water+ $\text{Al}_2\text{O}_3(0.1)$	Water+ $\text{Al}_2\text{O}_3(0.12)$	Water+ $\text{Al}_2\text{O}_3(0.14)$
HTC ($\text{kW}/\text{m}^2 \cdot \text{K}$)	0.85385	0.83064	0.937793	0.84058	0.8142	0.9186178
$q''(\text{kW}/\text{m}^2)$	81.107	78.9025	89.081	79.847	77.341	87.2595
$V(\text{m}/\text{s})$	0.124750	0.0096145	0.004878	0.0044828	0.0049	0.003978
$P(\text{Pascal})$	183.492	189.35	192.6566	195.2791	196.050	198.42377
$CP(\text{J}/\text{kg} \cdot \text{K})$	4179	4168.038	4157.076	4142.46	4135.1	4127.8442
$k(\text{W}/\text{m} \cdot \text{K})$	0.613	0.608	0.60309	0.5965501	0.59329	0.590052
$\rho(\text{kg}/\text{m}^3)$	999	1005.919	1014.83	1026.73	1032.67	1038.6219

Figure 5, Figure 6, Figure 7, Figure 8, Figure 9 and Figure 10 show counters from the Fluent program for some properties of the same concentrations of nanofluid Al_2O_3 +water. At low concentrations, nanofluids may not exhibit a significant enhancement in thermal conductivity due to insufficient nanoparticle dispersion. Conversely, at high concentrations, nanoparticle agglomeration can occur, leading to reduced effectiveness or even detrimental effects on heat transfer. The 0.6% volume concentration represents a balance between nanoparticle dispersion and aggregation. At this concentration, the nanoparticles are adequately dispersed within the base fluid, enhancing its thermal conductivity without excessive agglomeration. As a result, the nanofluid exhibits optimal heat transfer performance.

In Figure 11, concentration and heat flux are shown on surfaces with triangular, circular and square fins.

It's noted that the best concentration used of (Al_2O_3 +water) nanofluid was (0.6% volume) with the surfaces with circular fins having a percentage of (136%).

In Figure 12, concentration and HTC are shown on surfaces with triangular, circular, and square fins.

4.2 Geometrical Shapes of Fins

Three types of surfaces were used in this study that contain different geometric shapes of the fins:

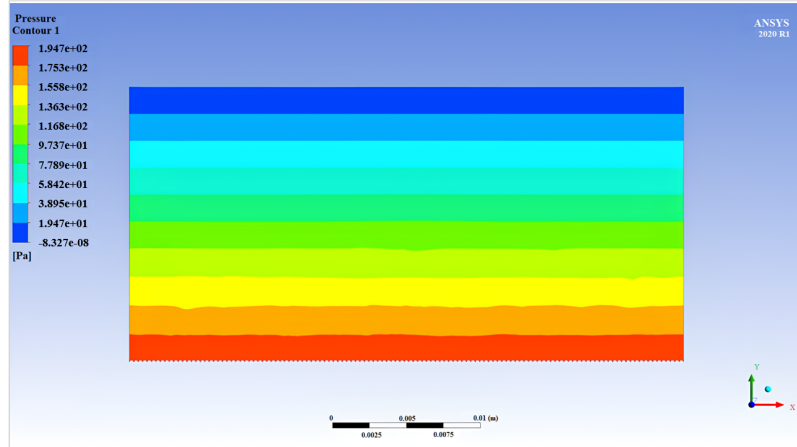


Figure 5. Contour of pressure for $\text{Al}_2\text{O}_3+\text{water}$ at concentration 0.6% vol. with square fins

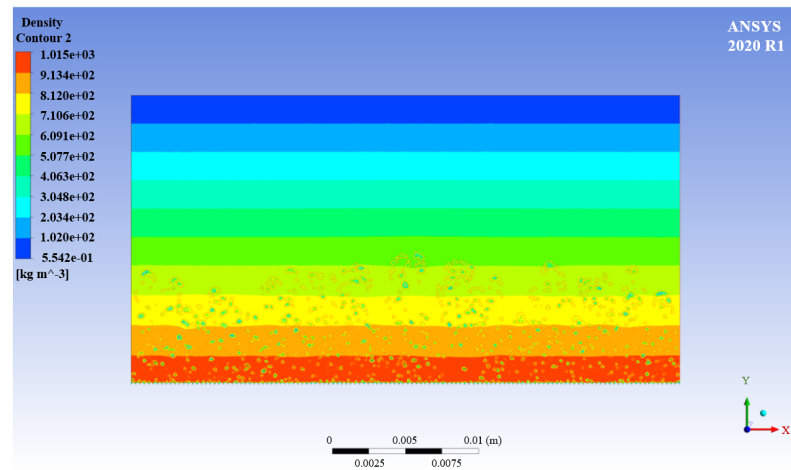


Figure 6. Contour of density for $\text{Al}_2\text{O}_3+\text{water}$ at concentration 0.6% vol. with circular fins

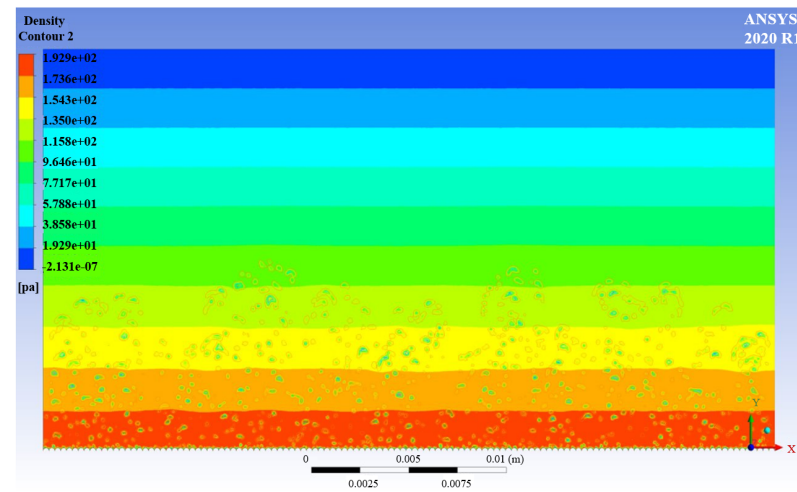


Figure 7. Contour of pressure for $\text{Al}_2\text{O}_3+\text{water}$ at concentration 0.6% vol. with circular fins

4.2.1 Triangular fins

- (1) The surfaces having triangular fins with a length of the base and a height of the triangle of 0.3 mm.
 - (2) In this study, (150774) nodes and (74669) elements are adopted.
- In Figure 13, the HTC on the surface with triangular fins shape are shown with ($\text{Al}_2\text{O}_3+\text{water}$) nanofluid.

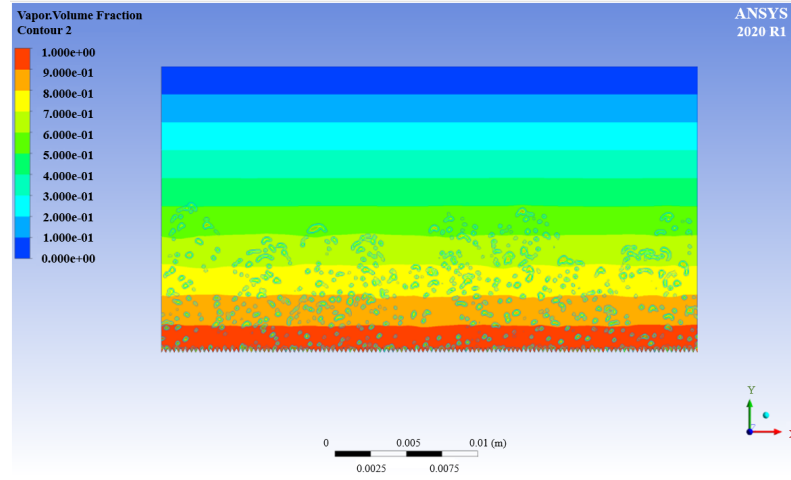


Figure 8. Contour of vapor volume fraction for Al_2O_3 +water at concentration 0.3% vol. with triangular fins

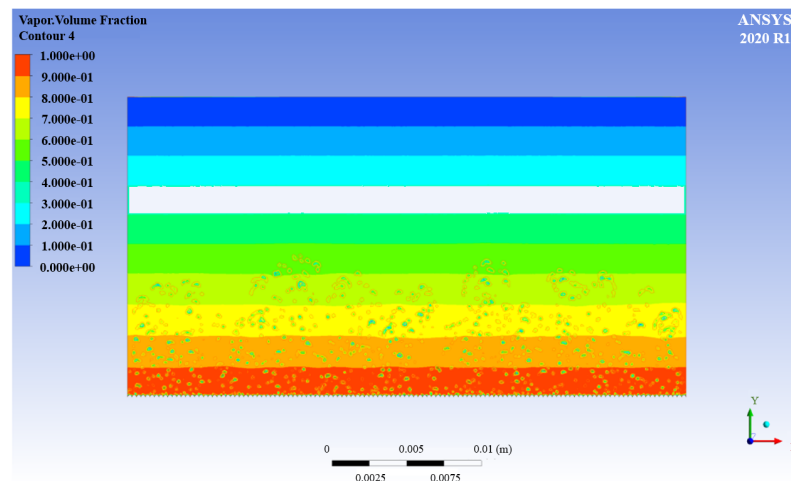


Figure 9. Contour of vapor volume fraction for Al_2O_3 +water at concentration 0.3% vol. with circular fins

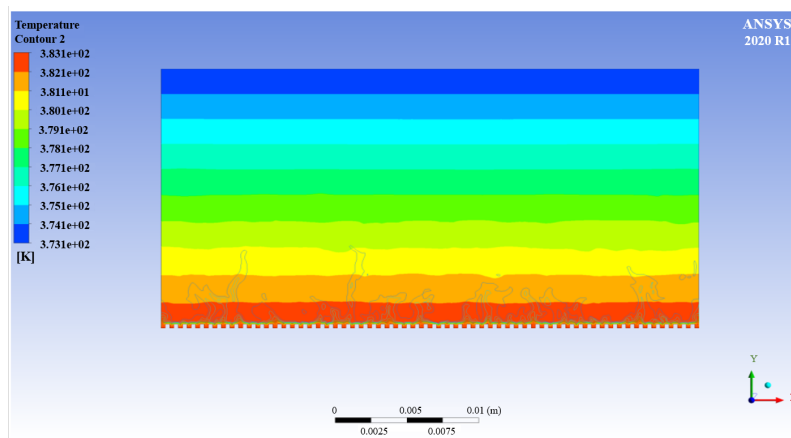


Figure 10. Contour of temperature for Al_2O_3 +water at concentration 0.3% vol. with square fins

4.2.2 Square fins

- (1) The surface having square fins with dimensions of 0.30 mm×0.30 mm.
- (2) In this study, (150408) nodes and (74442) elements are adopted.

In Figure 14, the HTC on the surface with square fins shape are shown with (Al_2O_3 +water) nanofluid.

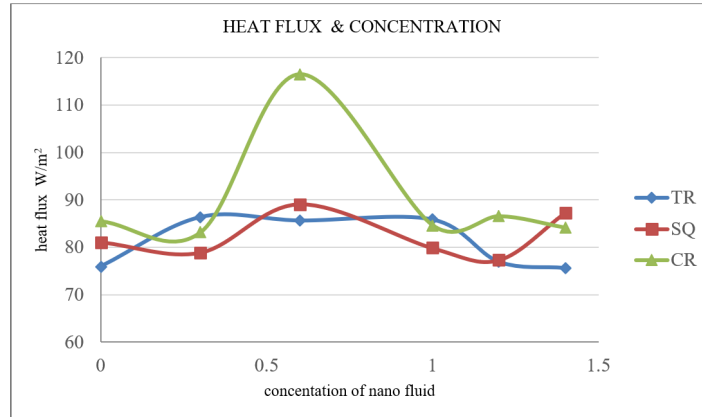


Figure 11. Different concentrations of (Al_2O_3 +water) on finned surfaces with square, circular and triangular geometric shapes

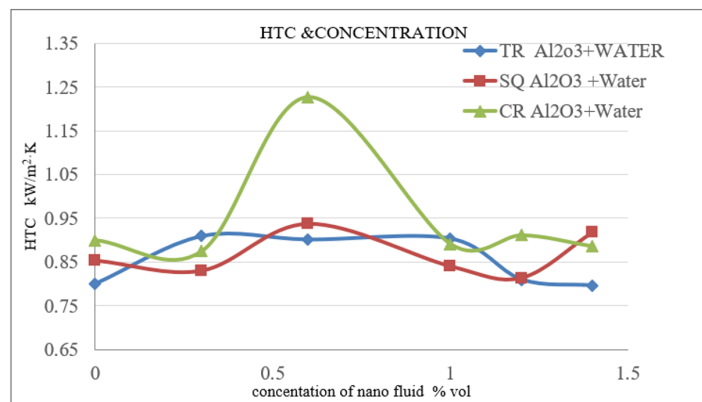


Figure 12. The different concentrations of the (Al_2O_3 +water) on the fins surfaces triangular, circular and square fins

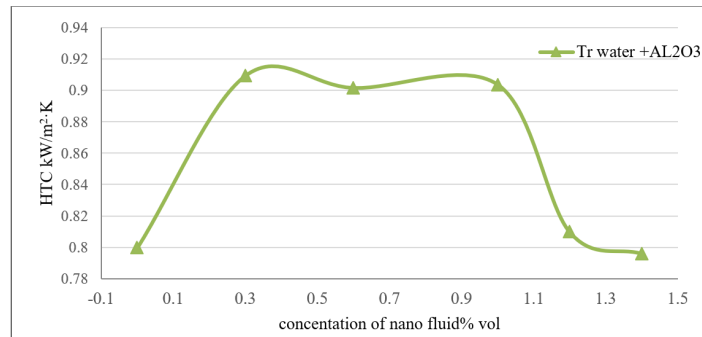


Figure 13. The different concentrations of the (Al_2O_3 +water) nanofluid on the surfaces with triangular geometric shapes of fins

4.2.3 Circular fins

- (1) The surfaces having circular fins with a diameter of 0.3 mm.
- (2) In this study, (161978) nodes and (159945) elements are adopted.

In Figure 15, the HTC on the surface with circular fins shape are shown with Al_2O_3 +water nanofluid.

The circular shapes of the fins had the best results for HTC with Al_2O_3 +water nanofluid at a concentration of 0.6% vol. and an amount of 1226.3 W/m² · K with a percentage of 136%.

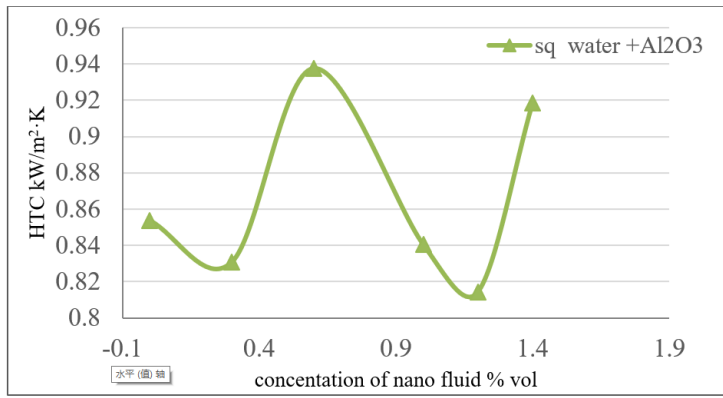


Figure 14. The different concentrations of the (Al_2O_3 +water) nanofluid on the surfaces with square geometric shapes of fins

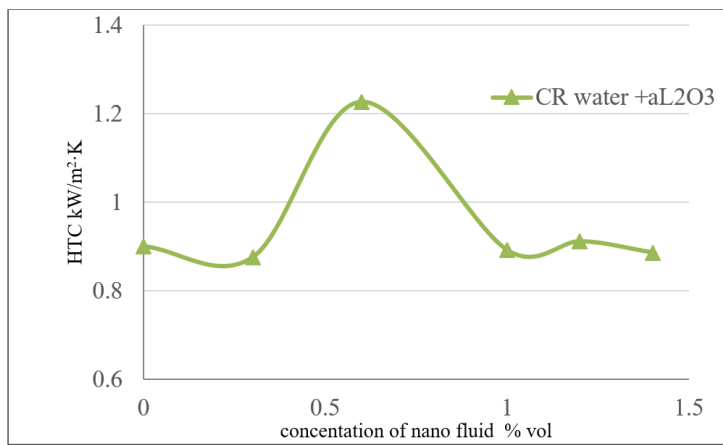


Figure 15. The different concentrations of the (Al_2O_3 +water) nanofluid on the surfaces with circular geometric shapes of fins

4.3 Different Fins Shape

The base fluid (water) is used in cooling transfer and heat transfer processors. In Figure 16, HTC on the surface with different of fins shapes are shown with (Al_2O_3 +water) nanofluid.

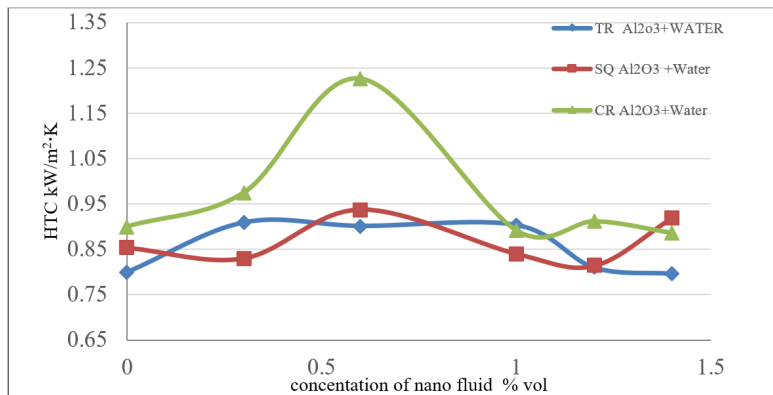


Figure 16. The different concentrations of the (Al_2O_3 +water) nanofluid on the different surfaces' shapes of fins

The circular shapes of the fins had the best results for HTC with Al_2O_3 +water nanofluid at a concentration of 0.6% vol. with a percentage of 136%.

5 Conclusions and Recommendations

This work investigates the synergistic results of utilizing nanofluids and micro-finned surfaces to enhance pool boiling heat transfer. Water-primarily-based Al₂O₃ nanofluids had been employed, with Al₂O₃ nanoparticles dispersed in the base fluid. Additionally, micro-finned surfaces were incorporated to enhance the available surface area for heat transfer. The research found numerous significant advantages associated with this mixed method. First, adding Al₂O₃ nanoparticles to the water-based fluid made it much better at conducting heat, which made it easier for heat to move around inside the fluid. Moreover, micro-finned surfaces provided extended surface locations, promoting more efficient heat dissipation at some point during pool boiling. Moreover, using nanofluids resulted in stronger wettability of the surface, in addition to improving the contact between the boiling liquid and the surface, which is crucial for efficient heat transfer. These mixed upgrades led to a sizable growth in heat transfer coefficients and a reduction in the CHF. However, it was also determined that the stability and long-term performance of nanofluids may be prompted by factors such as nanoparticle aggregation and sedimentation. However, the overall benefits of using nanofluids and micro-finned surfaces were greater than the drawbacks. This shows that this method can improve heat transfer in different thermal control programs for pool boiling. Further studies are warranted to optimize the layout parameters and address the demanding situations associated with long-term nanofluid stability.

The results show that surfaces with circular fins had, in general, the best results in the basic liquid, water. It was also found that the best concentrations of Al₂O₃+water nanofluid were 0.6% volume on surfaces with square fins and circular fins, while on surfaces with triangular fins, the best results were at a concentration of 0.3% volume.

It is recommended to use fluid flow instead of pool boiling with varying surfaces, fin shapes, and different types of nanofluids. Also, using microfin surfaces in numerical simulations involving several nanofluid types.

Data Availability

The data used to support the research findings are available from the corresponding author upon request.

Conflicts of Interest

The authors declare no conflict of interest.

References

- [1] H. Salehi and F. Hormozi, “Prediction of Al₂O₃-water nanofluids pool boiling heat transfer coefficient at low heat fluxes by using response surface methodology,” *J. Therm. Anal. Calorim.*, vol. 137, pp. 1069–1082, 2019. <https://doi.org/10.1007/s10973-018-07993-w>
- [2] M. Bahrami, *Forced Convection Heat Transfer*. Simon Fraser University, Burnaby, Canada, 2009.
- [3] E. Strak, R. Pastuszko, R. Kłosowiak, and R. Urbaniak, “Study of heat transfer during pool boiling on minifins surface coated with carbon nanotubes,” *Trans. Inst. Fluid-Flow Mach.*, no. 128, pp. 59–72, 2015.
- [4] M. M. Rahman and M. McCarthy, “Boiling enhancement on nanostructured surfaces with engineered variations in wettability and thermal conductivity,” *Heat Transf. Eng.*, vol. 38, no. 14-15, pp. 1285–1295, 2017. <https://doi.org/10.1080/01457632.2016.1242961>
- [5] S. C. S. Kumar, C. H. Yu, M. R. M. Arenales, A. Joseph, and P. H. Chen, “Effect of hydrophobic inclined patterns on pool boiling performance of cylindrical copper surfaces,” *Heat Mass Transf.*, vol. 56, no. 5, pp. 1379–1389, 2020. <https://doi.org/10.1007/s00231-019-02796-7>
- [6] H. Kim, G. DeWitt, T. McKrell, J. Buongiorno, and L. W. Hu, “On the quenching of steel and zircaloy spheres in water-based nanofluids with alumina, silica, and diamond nanoparticles,” *Int. J. Multiph. Flow*, vol. 35, no. 5, pp. 427–438, 2009. <https://doi.org/10.1016/j.ijmultiphaseflow.2009.02.004>
- [7] D. Ciloglu and A. Bolukbasi, “The quenching behavior of aqueous nanofluids around rods with high temperature,” *Nucl. Eng. Des.*, vol. 241, no. 7, pp. 2519–2527, 2011. <https://doi.org/10.1016/j.nucengdes.2011.04.023>
- [8] E. Akbari, A. M. Gheithaghy, H. Saffari, and S. M. Hosseinalipour, “Effect of silver nanoparticle deposition in re-entrant inclined minichannel on bubble dynamics for pool boiling enhancement,” *Exp. Therm. Fluid Sci.*, vol. 82, pp. 390–400, 2017. <https://doi.org/10.1016/j.expthermflusci.2016.11.037>
- [9] L. J. Habeeb, F. A. Saleh, and B. M. Maajel, “CFD modeling of laminar flow and heat transfer utilizing Al₂O₃/water nanofluid in a finned-tube with twisted tape,” *FME Trans.*, vol. 47, no. 1, pp. 89–100, 2019. <https://doi.org/10.5937/fmet1901089H>
- [10] A. N. A. Saied, M. A. Mashkour, H. M. Hussain, and L. J. Habeeb, “Numerical investigations of multiphase pool boiling in microchannels with several cooling materials,” *J. Mech. Eng. Res. Dev.*, vol. 44, no. 3, pp. 219–230, 2021. [https://jmerd.net/Paper/Vol.44,No.3\(2021\)/219-230.pdf](https://jmerd.net/Paper/Vol.44,No.3(2021)/219-230.pdf)
- [11] M. A. Mustafa, A. R. Abdullah, W. K. Hasan, L. J. Habeeb, and M. F. Nassar, “Two-way fluid-structure interaction study of twisted tape insert in a circular tube having integral fins with nanofluid,” *East. Eur. J. Enterp. Technol.*, vol. 3, no. 8, p. 111, 2021. <https://doi.org/10.15587/1729-4061.2021.234125>

- [12] H. H. Fadhl, A. Danch-Dezfuli, and L. J. Habeeb, “Pool boiling heat transfer enhancement using nano-fluids with ethylene-glycol base fluid and micro finned surface,” *Int. J. Multidiscip. Sci. Adv. Technol.*, vol. 3, no. 1, pp. 26–39, 2022. <https://drive.google.com/file/d/19axp5BG1ApmW6G2IdJf2DAkrSTa8Wjk8/view>
- [13] H. S. Majdi, H. M. A. Hussein, L. J. Habeeb, and D. Zivkovic, “Pool boiling simulation of two nanofluids at multi concentrations in enclosure with different shapes of fins,” *Mater. Today Proc.*, vol. 60, pp. 2043–2063, 2022. <https://doi.org/10.1016/j.matpr.2022.01.290>
- [14] K. Z. Zarrag, F. B. Ismail, T. E. Sann, and L. J. Habeeb, “A review of nucleate pool-boiling heat transfer in different liquids and nanofluids,” *Proc. Inst. Mech. Eng. Part A: J. Power Energy*, vol. 237, no. 7, pp. 1628–1641, 2023. <https://doi.org/10.1177/09576509231174692>
- [15] V. Guichet, S. Almahmoud, and H. Jouhara, “Nucleate pool boiling heat transfer in wickless heat pipes (two-phase closed thermosyphons): A critical review of correlations,” *Therm. Sci. Eng. Prog.*, vol. 13, p. 100384, 2019. <https://doi.org/10.1016/j.tsep.2019.100384>
- [16] ANSYS, Inc. (2013) ANSYS CFX Tutorials. http://iepoi.fs.um.si/upload/editor/lesnik/tutoriali_manuali/ANSYS%20CFX%20Tutorials.pdf